Journal of Molecular Catalysis A: Chemical 360 (2012) 35–41

Journal of Molecular Catalysis A: Chemical

journal homepage: www.elsevier.com/locate/molcata

The choice of precipitant and precursor in the co-precipitation synthesis of copper manganese oxide for maximizing carbon monoxide oxidation

Li-Na Cai [a], Yue Guo [a], An-Hui Lu [a], Peter Branton [b], Wen-Cui Li [a,*]

[a] The State Key Laboratory of Fine Chemicals, School of Chemical Engineering, Dalian University of Technology, Dalian 116024, PR China
[b] Group Research & Development Centre, British American Tobacco, Regents Park Road, Southampton SO15 8TL, UK

ARTICLE INFO

Article history:
Received 23 February 2012
Received in revised form 3 April 2012
Accepted 4 April 2012
Available online 11 April 2012

Keywords:
Copper manganese oxide
Co-precipitation
Precursor
Precipitant
CO oxidation

ABSTRACT

Copper manganese oxides (CMOs) were synthesized using a co-precipitation method with different precursors and precipitants for carbon monoxide oxidation. The as-synthesized catalysts were characterized by powder X-ray diffraction (XRD), low temperature N_2 sorption, Fourier transform-infrared spectroscopy (FT-IR), H_2-temperature programmed reduction (H_2-TPR), and thermal gravimetric analysis (TGA). Their catalytic activities for CO oxidation were tested by temperature programmed reaction. The results showed that the activity of CO oxidation strongly depended on the combination of precipitant and precursor anions, ranking in the order $(Ac^- + CO_3^{2-}) > (NO_3^- + CO_3^{2-}) > (Ac^- + OH^-) > (NO_3^- + OH^-)$. The crystalline phase of copper manganese oxides obtained using strong electrolyte (OH^-) as the precipitant were mainly spinel $Cu_{1.5}Mn_{1.5}O_4$, while the catalysts prepared with weak electrolyte (CO_3^{2-}) as the precipitant mostly comprised of $MnCO_3$, Mn_2O_3 and CuO, and showed a much higher CO oxidation activity than that of the $Cu_{1.5}Mn_{1.5}O_4$. Keeping the same precipitant while changing the precursor caused a change in the H_2 consumption which influenced the CO oxidation activity. A suitable combination of precipitant and precursor resulted in the most efficient CO oxidation catalyst.

1. Introduction

Catalytic oxidation of carbon monoxide receives considerable attention due to its many applications in industry and environmental fields, such as CO_2 laser gas generation, personal respiratory protective devices, proton exchange membrane fuel cells and automobile emission controls [1–8]. Since Haruta's report on the unexpectedly high catalytic activity of supported gold nanoparticles with a size below 5 nm [9], various catalysts based on noble metal nanoparticles have been developed to oxidize carbon monoxide [10–16]. However, the high cost of noble metal catalysts inhibits their practical applications for the catalytic oxidation of carbon monoxide. Compared to noble metal catalysts, copper manganese oxide, one of the oldest known catalysts used in respiratory protection, also shows a relatively high CO oxidation activity [17,18] and is considered to be a potential candidate for substituting noble metal catalysts for CO oxidation for certain applications [19–27].

To date, numerous methods have been established to synthesize copper manganese oxide catalysts, including co-precipitation sol–gel, ultrasonic aerosol pyrolysis, supercritical antisolvent precipitation and reduction methods [1,28–31]. Among these methods, conventional co-precipitation can be used to produce catalysts with improved activity. Hutchings and co-workers have investigated the effect of the preparation conditions in the co-precipitation process and subsequent calcination step on the catalytic performance of copper manganese oxide catalysts for CO oxidation [32–34]. It was found that ageing time and calcination temperatures have an important influence on the crystalline phase of the copper manganese oxide catalysts. Without the ageing step, the precipitate is composed of crystalline copper hydroxy nitrate together with manganese carbonate. With an increasing ageing time, the copper hydroxy nitrate re-dissolves and poorly crystalline manganese carbonate is identified. Thus, the state of the precipitate varies depending on the ageing time, which results in the formation of calcined catalysts with different crystalline phases and different catalytic performance. In the calcination process, the crystallinity is lost with increasing calcination temperature, with gradual transformation to amorphous copper manganese oxide. However, when the calcination temperature reaches 400 °C, the microcrystalline $CuMn_2O_4$ hopcalite phase is formed.

The exact phase responsible for the high catalytic activity in copper manganese oxide is still disputed. One hypothesis is that the high activity is due to the formation of the copper-manganese spinel $CuMn_2O_4$ formed during co-precipitation. The redox reaction $Cu^{2+} + Mn^{3+} = Cu^{1+} + Mn^{4+}$ has been proposed to explain the activity, *i.e.* an electronic transfer between copper and manganese cations within the spinel lattice [28,35]. Another hypothesis attributes the high oxidation activity at room temperature to the so

* Corresponding author. Fax: +86 411 84986140.
E-mail address: wencuili@dlut.edu.cn (W.-C. Li).

1381-1169
http://dx.doi.org/10.1016/j.molcata.2012.04.003

called 'amorphous' copper manganese oxide instead of the spinel $CuMn_2O_4$ [36–39].

It seems reasonable to conclude that the phase structure of copper manganese oxide catalysts has a significant influence on the activity of CO oxidation. In the present study, different types of precipitants and precursors have been used in order to change the crystalline phase of the catalysts. Catalysts before and after CO oxidation have been characterized. The aim of the current study was to find the optimum combination of precipitant and precursor to give the catalyst with highest CO oxidation activity.

2. Experimental

2.1. Catalyst preparation

All the chemicals used in this study were of analytical grade and used without any further purification. The copper manganese oxide catalysts were prepared by co-precipitation of sodium carbonate (Na_2CO_3) or sodium hydroxide (NaOH) as the precipitant, and acetate or nitrate as the precursor. The typical procedure to synthesize the catalysts was as follows: a precipitant (9 mmol) was dissolved in deionized water (15 mL) with an initial pH value of *ca.* 13. Precursors (4.5 mmol) were mixed with deionized water (15 mL) with a 1/2 molar ratio of copper to manganese species. The mixed precursor solution was then added to the precipitant solution at 298 K under vigorous stirring. After 5 min, the final pH of the mixed solutions was adjusted to 11 using 4 mol/L NaOH solutions. The resultant suspensions were aged for 30 min under vigorous stirring at 298 K. Finally the precipitate was filtered, washed several times with deionized water and finally once with anhydrous alcohol, followed by drying in air at 50 °C for 24 h (denoted as $CuMO_x$-*X*, *X* = 1, 2, 3, 4) and calcination at 300 °C for 2 h (denoted as $CuMO_x$-*X*-C) to obtain the final catalysts. Detailed sample information is shown in Table 1. For comparison, the pure copper oxide and manganese oxide catalysts were synthesized separately by using the acetate as precursor and sodium carbonate (Na_2CO_3) or sodium hydroxide (NaOH) as the precipitant by keeping the other synthesis and after-treatment conditions the same as the copper manganese oxide. The corresponding samples were named as CuO-1-C (Na_2CO_3 as the precipitant), CuO-2-C (NaOH as the precipitant), MnO_x-1-C (Na_2CO_3 as the precipitant), MnO_x-2-C (NaOH as the precipitant), respectively. Detailed information of the comparison samples are also listed in Table 1.

2.2. Catalyst characterization

X-ray diffraction patterns (XRD) were obtained with a D/MAX-2400 diffractometer using Cu Kα radiation (40 kV, 100 mA, λ = 1.54056 Å). The textural characterizations of the samples were performed by nitrogen sorption at 77 K using a Micromeritics Instrument Corporation Tristar 3000 device. Approximately 200 mg samples were heated to 200 °C under vacuum for 4 h to remove all adsorbed species. The surface area (S_{BET}) and pore size distribution were calculated using the Brunauer–Emmett–Teller (BET) theory and Barrett–Joyner–Halendar (BJH) theory, respectively. The total pore volume (V_{total}) was estimated from the amount adsorbed at a relative pressure of 0.992. The micropore volume was determined using the *t*-plot method. The morphologies of the catalysts were characterized with a FEI Quanta 450 instrument microscope equipped and a cooled energy-dispersive X-ray (EDX) spectrometer from Oxford Instruments for point resolved elemental analysis. Fourier transform-infrared (FT-IR) spectra were recorded on a Nicolet 6700 FT-IR spectrometer with the samples pressed into KBr discs. Thermogravimetric analysis (TGA) was conducted on a thermogravimetric analyzer STA 449 F3 (NETZSCH), under an air atmosphere with a heating rate of 10 K/min. Temperature programmed reduction of hydrogen (H_2-TPR) was performed on a Micromeritics Auto Chem II 2920 apparatus with a thermal conductive detector by passing 8% H_2/Ar (flow rate of 50 mL/min) over a 20 mg sample (40–60 mesh size) at a heating rate of 10 K/min to 1173 K. Before H_2-TPR, the samples were pretreated with He at 473 K for 1 h to clear the surface of catalysts. The system was then cooled to ambient temperature under He. The amount of hydrogen consumed (H_2 cons.) by each catalyst was calculated from the peak area of the H_2-TPR profile.

2.3. Catalytic test

The activities of the copper manganese oxide catalysts for CO oxidation were measured in a quartz tubular fixed bed flow reactor at atmospheric pressure using 200 mg of catalyst (40–60 mesh). The standard composition of the feed gas was 1% CO, 20% O_2 and 79% N_2 with a space velocity of 20,000 mL h^{-1} g_{cat}^{-1}. The temperature was ramped at a rate of 1 °C min^{-1} from 0 °C to the final temperature. The concentrations of CO were analyzed at the outlet of the reactor by a GC 7890T gas chromatograph (Techcomp Limited Company, China) equipped with a thermal conductivity detector (TCD). Temperatures for 100% conversion of CO ($T_{100\%}$) and 50% conversion of CO ($T_{50\%}$) were used to evaluate the activity of the catalysts.

3. Results and discussion

3.1. Catalyst characterization

Table 1 summarized details of the catalysts synthesized. XRD analysis of the catalysts (Fig. 1) was used to determine the final phases after heat treatment at 300 °C in static air for 2 h. Clearly, the reflections of the both samples CuO-1-C and CuO-2-C can be assigned to CuO phases (JCPDS 45-0937). Nevertheless, the samples MnO_x-1-C and MnO_x-2-C show mixed diffraction lines of Mn_2O_3 (JCPDS No. 33-0900) and Mn_3O_4 (JCPDS No. 65-2776). In addition, the diffraction peaks of $MnCO_3$ (JCPDS No. 44-1472) also was observed in the sample MnO_x-1-C, which synthesized using sodium carbonate as a precipitant.

Samples $CuMnO_x$-1-C and $CuMnO_x$-3-C prepared with Na_2CO_3 as a precipitant present a low crystallinity but reflections of Mn_2O_3, CuO and $MnCO_3$ were detected. The $CuMnO_x$-2-C and $CuMnO_x$-4-C materials prepared with NaOH as a precipitant however mainly have a spinel $Cu_{1.5}Mn_{1.5}O_4$ (JCPDS No. 35-1171) structure following calcination at 300 °C. The crystallinity of the catalysts increased using by sodium hydroxide as the precipitant. In other words, different types of precipitants can influence the final crystalline phases of the catalysts.

Nitrogen sorption at 77 K was used to evaluate the pore structure of the catalysts. Fig. 2 shows the nitrogen sorption isotherms and the pore size distribution of the catalysts. According to the IUPAC classification, the N_2 sorption isotherms of all samples exhibit type IV characteristics as shown in Fig. 2(a). The existence of a hysteresis loop at relative pressure (P/P_0) of 0.8–1.0 indicates the porosity arising from the non-crystalline intra-aggregate voids and spaces formed by interparticle contacts [40]. Fig. 2(b) shows the pore size distributions (PSDs) as calculated by the Barrett–Joyner–Halendar (BJH) method from the desorption branch of the nitrogen isotherms. Samples $CuMnO_x$-1-C and $CuMnO_x$-3-C exhibited a smaller pore size than samples $CuMnO_x$-2-C and $CuMnO_x$-4-C, as a result of the different precipitants. The porous textural parameters, such as specific surface area (S_{BET}) and pore volume (V_{total}) are also listed in Table 1. It can be seen that using sodium carbonate instead of sodium hydroxide as a precipitant resulted in a higher specific surface area and total pore

Table 1
Information and characterization data for catalysts prepared with different precipitants and precursors.

Sample	Precursor	Precipitant	Crystalline phase	S_{BET} ($m^2\ g^{-1}$)	V_{total} ($cm^3\ g^{-1}$)	$T_{100\%}$ [a] (°C)	$T_{50\%}$ [b] (°C)	H_2 cons.[c] (mL/g)
$CuMnO_x$-1-C	$Cu(Ac)_2$ $Mn(Ac)_2$	Na_2CO_3	Mn_2O_3, CuO, $MnCO_3$	121	0.53	50	25	198.7
$CuMnO_x$-2-C	$Cu(Ac)_2$ $Mn(Ac)_2$	NaOH	$Cu_{1.5}Mn_{1.5}O_4$	70	0.36	110	72	209.4
$CuMnO_x$-3-C	$Cu(NO_3)_2$ $Mn(NO_3)_2$	Na_2CO_3	Mn_2O_3, CuO, $MnCO_3$	109	0.46	70	35	192.6
$CuMnO_x$-4-C	$Cu(NO_3)_2$ $Mn(NO_3)_2$	NaOH	$Cu_{1.5}Mn_{1.5}O_4$	46	0.23	120	80	183.2
CuO-1-C	$Cu(Ac)_2$	Na_2CO_3	CuO	–	–	130	115	300.2
CuO-2-C	$Cu(Ac)_2$	NaOH	CuO	–	–	140	120	266.7
MnO_x-1-C	$Mn(Ac)_2$	Na_2CO_3	Mn_2O_3, Mn_3O_4, $MnCO_3$	–	–	170	128	103.5
MnO_x-2-C	$Mn(Ac)_2$	NaOH	Mn_2O_3, Mn_3O_4	–	–	170	132	167.1

[a] Temperature of complete conversion of CO to CO_2.
[b] Temperature of 50% conversion of CO to CO_2.
[c] H_2 consumption was calculated through the integral of the corresponding peak areas.

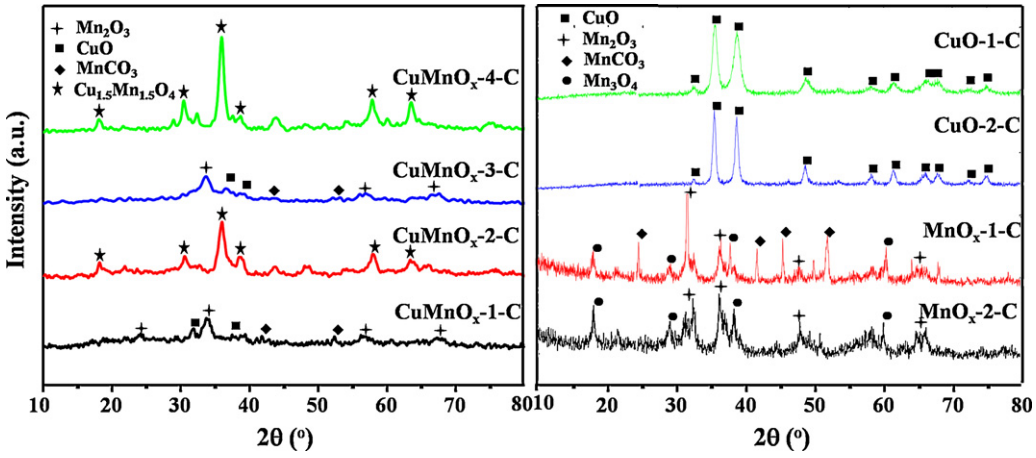

Fig. 1. XRD patterns of the catalysts prepared using different precursors and precipitants.

volume. Catalyst $CuMnO_x$-1-C prepared using Na_2CO_3 as a precipitant showed a specific surface area and pore volume of 121 $m^2\ g^{-1}$ and 0.53 $cm^3\ g^{-1}$ respectively. Specific surface area and total pore volume are two significant factors which can affect the catalytic performance for CO oxidation [39]. When the catalytic activity was tested (see later), it was found that the higher catalyst specific surface area and total volume resulted in the greatest catalytic activity.

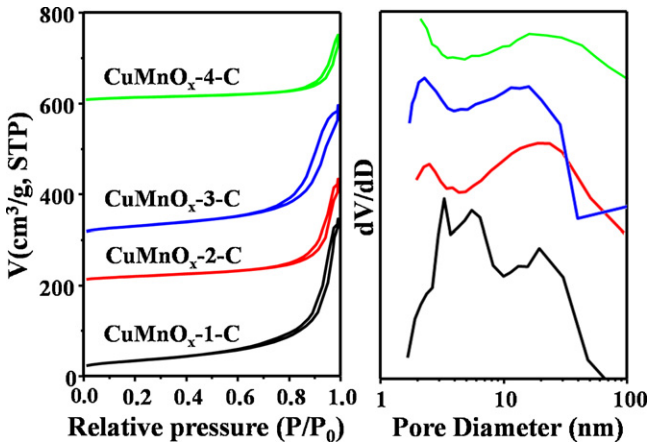

Fig. 2. Nitrogen sorption isotherms (a) and the corresponding pore size distributions (b) of the catalysts. The isotherms of $CuMnO_x$-2-C, $CuMnO_x$-3-C and $CuMnO_x$-4-C were offset vertically by 200, 300 and 600 $cm^3\ g^{-1}$, STP, respectively.

Furthermore, the samples were characterized by SEM equipped with EDX and the results are shown in Fig. 3. It can be seen that all the powder catalysts have similar morphologies which composed of irregular sized- and shaped-particles (Fig. 3(a)–(d)). The surface of catalysts displays abundant macropores probably accumulated with grains, which is confirmed by the nitrogen isotherm and pore size distributions in Fig. 2. All the catalysts have similar morphologies, indicating that the types of precipitants and precursors have weak influence on the catalyst morphologies.

In order to verify the atom ratio of copper to manganese of the catalysts, EDX analysis based SEM was performed in a large scanning range (200–700 μm) by random for the samples $CuMnO_x$-1-C, $CuMnO_x$-2-C, $CuMnO_x$-3-C, $CuMnO_x$-4-C, respectively, and the results are shown in Fig. 3(e)–(h). The presence of Cu, Mn and O on the surface of the samples can be clearly detected. The surface atom ratio of the catalysts prepared with different precipitants and precursors are compiled in Table 2. The Cu/Mn molar ratio of all the catalysts using co-precipitation method is approximately 0.5, which is very close to the actual dosage of copper and

Table 2
Surface atom ratios for catalysts prepared with different precipitants and precursors.

Sample	Atom ratio (%)			Cu/Mn molar ratio
	Cu	Mn	O	
$CuMnO_x$-1-C	6.16	11.37	82.47	0.542
$CuMnO_x$-2-C	12.17	24.60	63.23	0.495
$CuMnO_x$-3-C	10.43	23.43	66.14	0.445
$CuMnO_x$-4-C	12.42	25.12	62.46	0.494

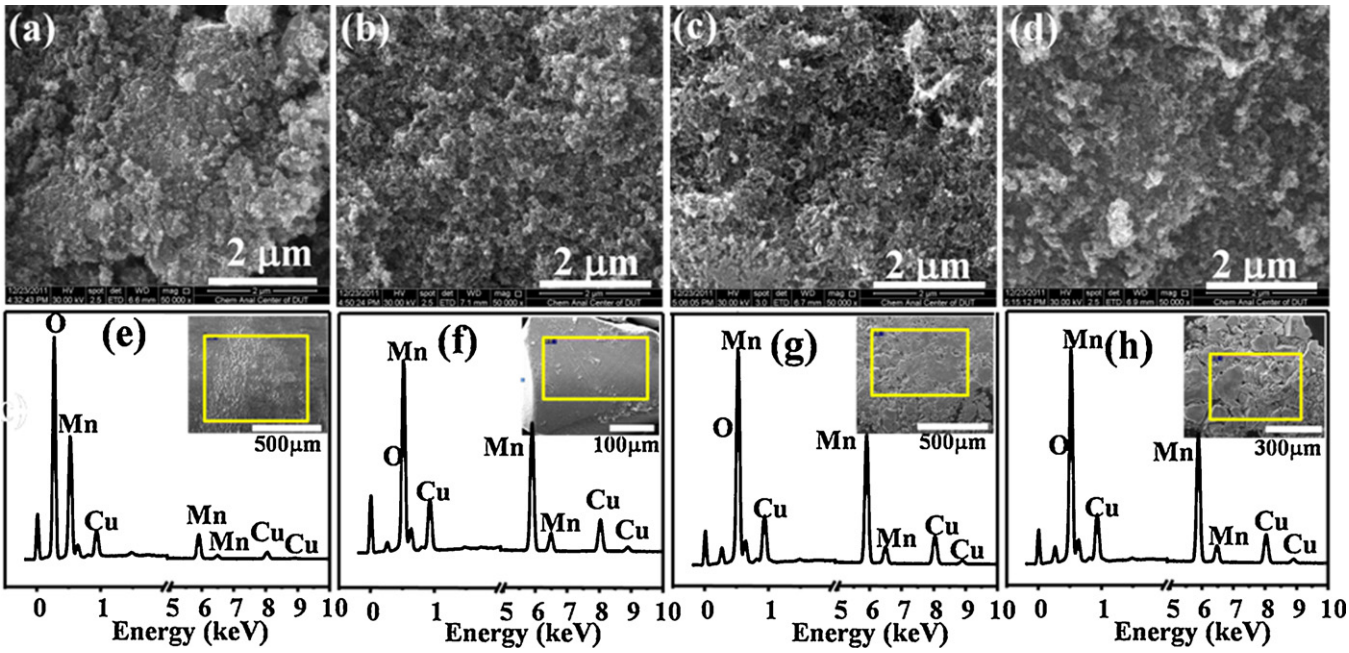

Fig. 3. SEM images and EDX of catalysts prepared with different precursors and precipitants: (a and e) $CuMnO_x$-1-C; (b and f) $CuMnO_x$-2-C; (c and g) $CuMnO_x$-3-C; (d and h) $CuMnO_x$-1-C.

manganese precursors. Notably, the relative atom ratio of O and Cu/Mn molar ratio for sample $CuMnO_x$-1-C are 82.47% and 0.542 (shown in Table 2), respectively, which are much higher than that of the other three catalysts. The abundant surface oxygen atoms of the catalyst can react with the absorbed CO and thus lead to better activity in the Mars–van Krevelen type mechanism (MvK) [41] which is frequently suggested for metal-oxides. The choice of the different precursor and precipitant leads to the change of the surface distribution of Cu, Mn and O elements, which might be related to the CO oxidation catalytic performance of the catalysts.

3.2. Catalytic performance of the copper manganese oxides for CO oxidation

The performance of the catalysts for CO oxidation is shown in Fig. 4. The determined $T_{50\%}$ (temperature for 50% CO conversion) and $T_{100\%}$ (temperature for 100% CO conversion) are listed in Table 1. As seen in Fig. 4, pure copper oxides CuO-1-C, CuO-2-C and pure manganese oxides MnO_x-1-C, MnO_x-2-C prepared using acetates as precursors show quite similar catalytic activities in the low temperature range. Their corresponding conversion could not achieve 10% until the temperature reaches 80 °C. At higher temperatures the conversions over pure copper oxides rise strongly and a complete conversion can be reached at 120–140 °C.

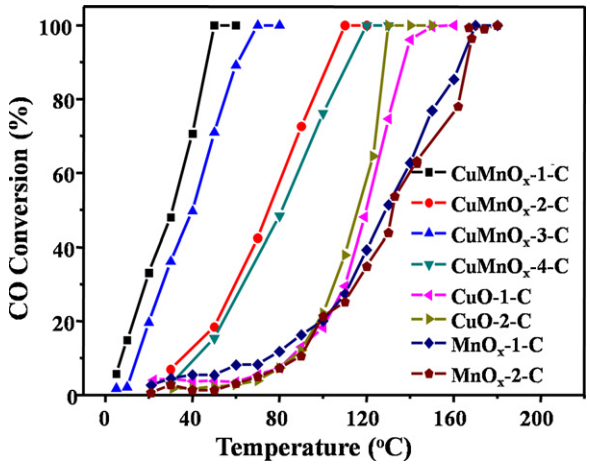

Fig. 4. Catalytic performance of catalysts, 200 mg catalyst, and space velocity: 20,000 mL h^{-1} g_{cat}^{-1}, and feed gas: 1% CO, 20% O_2 and 79% N_2.

The activity of the copper manganese oxides catalysts is significantly improved, especially at low-temperature range. The catalyst synthesized using acetate and Na_2CO_3 ($CuMnO_x$-1-C) showed the greatest CO oxidation activity, where 50% conversion of CO ($T_{50\%}$) and complete conversion of CO ($T_{100\%}$) was achieved at 25 °C and 50 °C respectively. Using the same precursor, the catalysts prepared with carbonate as the precipitant were considerably more active than catalysts prepared with NaOH as the precipitant. In other words the activities of the multiphase catalysts CuO and Mn_2O_3 were several times higher than those of single phase oxides ($Cu_{1.5}Mn_{1.5}O_4$), especially in the lower temperature range. It has been previously reported that the coordination between copper and manganese oxides improves the catalyst CO oxidation activity [38]. It was found that, the precipitant could lead to different crystalline phase formation of the catalysts. Copper manganese mixed oxides show the higher catalytic activity than that of spinal $Cu_{1.5}Mn_{1.5}O_4$. The results obtained in this work show that precipitants had a significant impact on the crystalline phases of catalysts and CO oxidation activity. However, there are slight differences between catalysts synthesized with the same precipitant.

The results showed that the activity of CO oxidation strongly depended on the combination of precipitant and precursor anions, ranking in the order $(Ac^- + CO_3^{2-}) > (NO_3^- + CO_3^{2-}) > (Ac^- + OH^-) > (NO_3^- + OH^-)$. With the same precipitant, the catalysts prepared with acetate as a precursor resulted in a better catalytic activity than that of prepared with nitrates as a precursor. As reflected in EDX analysis (Table 2), the combination of acetate and carbonate results in an oxygen-rich surface for sample $CuMnO_x$-1-C and accordingly a higher CO oxidation activity. The XRD analysis of the used catalysts ($CuMnO_x$-1-C and $CuMnO_x$-3-C samples) was carried out (Fig. 5). It can be seen that the used catalysts showed a very similar XRD curves as catalysts before test, demonstrating that CuO and Mn_2O_3 underwent little

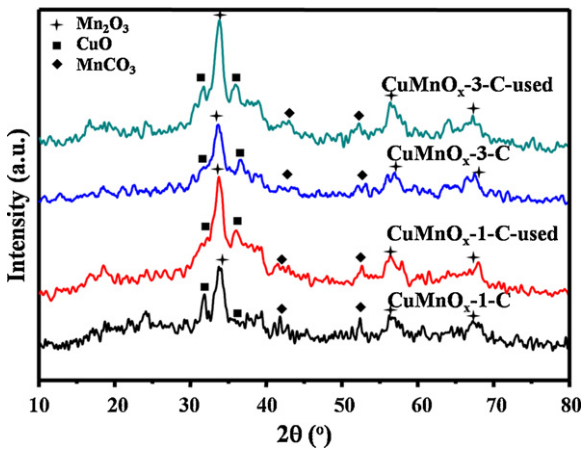

Fig. 5. XRD patterns of the catalysts before and after using.

phase change during the catalytic test and should be the active phase for CO oxidation. Combination with the following H_2-TPR, the coexistence of Mn_2O_3 and CuO phases is essential for the higher activity.

H_2-TPR measurements on freshly calcined samples were carried out (Fig. 6) to investigate the reduction properties of different samples. The reduction of pure copper oxides CuO-1-C and CuO-2-C occurs in one step that probably corresponds to the reduction of CuO to Cu^0 at the temperature peak of 205 and 196 °C, respectively. The TPR profiles of pure manganese oxides MnO_x-1-C and MnO_x-2-C exhibit two peaks. The first one at 234 and 247 °C can be assigned to the reduction of Mn_2O_3 to Mn_3O_4, and the second reduction peak at 402 and 383 °C should be the transformation of Mn_3O_4 to MnO, respectively [38]. For pure copper or manganese oxides, the choice of precipitants either carbonate or hydroxide do not exert big influence on the reduction ability, which is coincident with the catalytic activity results.

The reduction peaks of sample $CuMnO_x$-1-C and $CuMnO_x$-3-C are quite wide and overlapped, which is hard to precisely identify each peak. The curves of samples *CuMnO*$_x$-1-C and $CuMnO_x$-3-C, which mainly consist of Mn_2O_3 and CuO, show four peaks. In this work, the first two peaks at low temperatures (100–110 °C and 155–176 °C) are assigned to the reduction of the highly dispersed and bulky CuO, respectively [42]. The other two peaks can be assigned to the reduction of manganese oxide (Mn_2O_3 to Mn_3O_4 and Mn_3O_4 to MnO) [43]. The temperature of the first peak is *ca.* 100 °C, which is considerably lower than that of pure copper oxide. The presence of manganese oxide is likely to facilitate the reduction of copper oxide, involving coordination between CuO and Mn_2O_3 with manganese oxide acting as oxygen donor and copper oxide as oxygen acceptor [38]. Previous work demonstrated that the presence of Cu^{2+} and Mn^{3+} is essential for the high activity of the catalyst [44]. Catalysts $CuMnO_x$-2-C and $CuMnO_x$-4-C however have only one peak due to the reduction of the spinel phase $Cu_{1.5}Mn_{1.5}O_4$. This result is consistent with a previous study where the higher temperature reduction peaks disappear when the copper manganese oxide has the formula $Cu_{1+x}Mn_{2-x}O_4$ ($x = 0.54 \pm 0.04$) [33]. It should be noted that only $Cu_{1.5}Mn_{1.5}O_4$ can be observed in the XRD patterns and the surface Cu/Mn ratio is ~2 as determined from EDX results. This indicates the existence of amorphous manganese oxides, which can be reduced at the same temperature range as that of $Cu_{1.5}Mn_{1.5}O_4$. The asymmetric reduction peaks in TPR curves of $CuMnO_x$-2-C and $CuMnO_x$-4-C were observed, attributing to the peaks overlapping resulting from the mixed oxides [45]. Although synthesized with the same acetate precursor, the temperature of the first peak of sample $CuMnO_x$-1-C is considerably lower than that of the sample $CuMnO_x$-2-C, which suggests that the coexistence of Mn_2O_3 and CuO phases is essential for the higher activity. The results are similar with samples prepared with nitrate as a precursor. It can be concluded that samples synthesized with carbonate as a precipitant possess a higher reducibility which shows a greater CO oxidation activity than that synthesized with NaOH as the precipitant.

H_2 consumption was calculated through the integral of the corresponding peak areas (Table 1). Although sample $CuMnO_x$-1-C and $CuMnO_x$-3-C (copper manganese mixed oxide) showed a less H_2 consumption compared to the sample $CuMnO_x$-2-C ($Cu_{1.5}Mn_{1.5}O_4$ spinel), H_2-TPR profiles showed that the reduction temperature of sample $CuMnO_x$-1-C and $CuMnO_x$-3-C is much lower than the sample $CuMnO_x$-2-C. The TPR peaks at lower temperature usually can be related with the catalytic activity [46]. For the sample $CuMnO_x$-1-C and $CuMnO_x$-3-C, the temperature of their first peak is similar; however $CuMnO_x$-1-C shows greater hydrogen consumption than that of $CuMnO_x$-3-C, corresponding to a relatively high activity. Similarly, $CuMnO_x$-2-C shows greater hydrogen consumption than that of $CuMnO_x$-4-C. Therefore, for catalysts with different phase structure, the reduction temperature is mainly related to activity, for catalysts with same phase structure, the H_2 consumption can be used to evaluate the activity difference. Based on H_2 consumption result, it can be more or less concluded, when using the same precipitant, samples prepared with acetate as a precursor show a

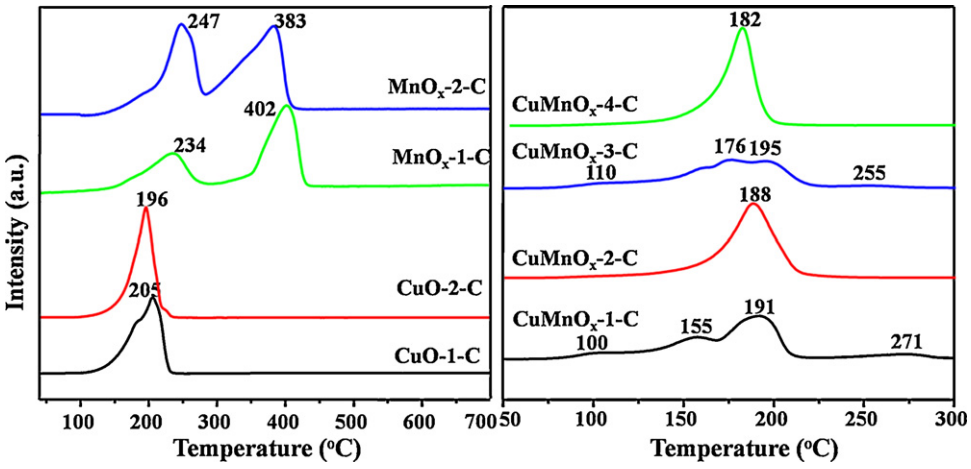

Fig. 6. TPR profiles of catalysts prepared with different precursors and precipitants.

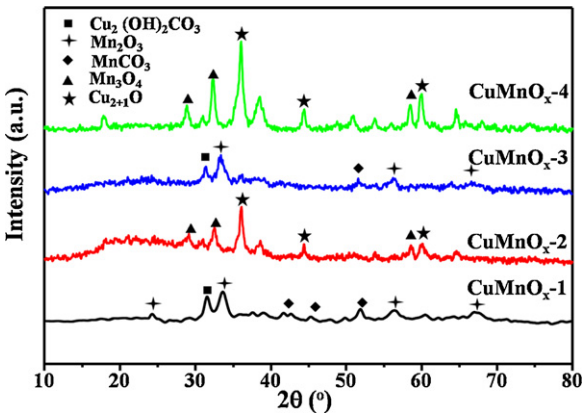

Fig. 7. XRD patterns of the dried precipitates prepared by different precursors and precipitants.

higher reduction activity than samples prepared with nitrate as the precursor.

3.3. Insight into the interactions between precursor and precipitant

To demonstrate how the significantly different crystalline phases of the as-synthesized catalysts prepared with dissimilar types of alkali influence the CO oxidation activity, FT-IR, XRD and TGA of the dried samples were performed.

An XRD analysis was used to further ascertain the compositions of the dried samples prior to calcination. The corresponding wide-angle XRD patterns of the precipitation prepared using different precursors and precipitants after drying at 50 °C are shown in Fig. 7. As can be seen, all the dried samples have distinct diffraction peaks, which is consistent with the fact that they all exist in the crystalline phase. $CuMnO_x$-1 and $CuMnO_x$-3 predominantly consist of $Cu_2(OH)_2CO_3$, $MnCO_3$ and Mn_2O_3 derived from the $MnCO_3$ (which is susceptible to oxidation in wet environments). $Cu_{2+1}O$ (JCPDS 05-0667) and Mn_3O_4 (JCPDS 80-0382) phases mainly present in $CuMnO_x$-2 and $CuMnO_x$-4 are converted to $Cu_{1.5}Mn_{1.5}O_4$ after calcination at 300 °C. This process is likely to be the isomorphism substitution of the Mn^{3+} and Mn^{4+} in the Mn_3O_4 with Cu^+ or Cu^{2+} from $Cu_{2+1}O$ [47].

FT-IR was performed to identify the functional groups of the dried samples. Fig. 8 shows the FT-IR spectra of the dried samples prior to calcination. All samples show a well-defined band

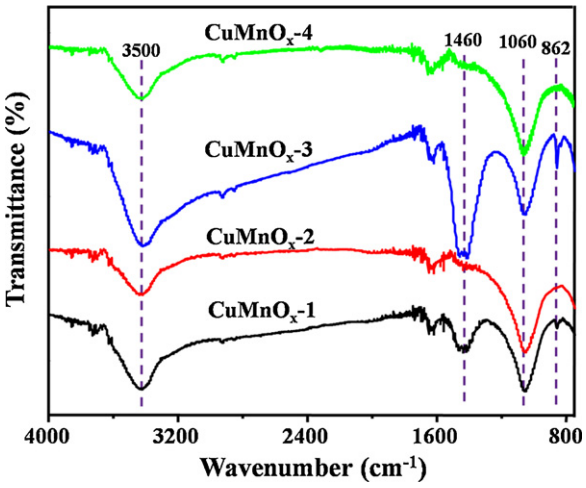

Fig. 8. FT-IR curves of catalysts prepared with different precursors and precipitants.

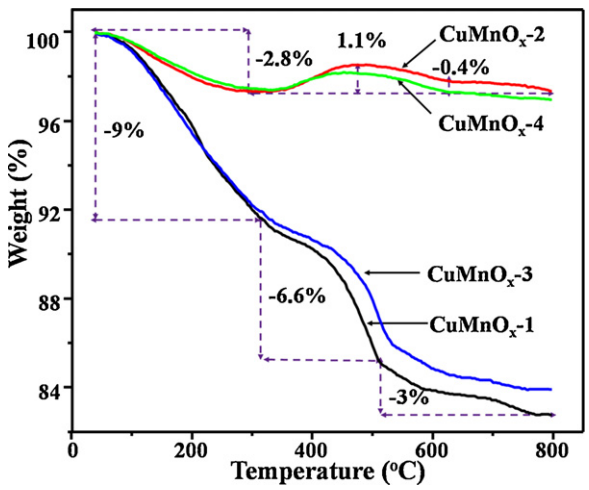

Fig. 9. TGA curves of the precipitates prepared with different precursors and precipitants.

at 3500 cm^{-1} which can be attributed to the hydroxyl stretching vibration, indicating that hydroxide precipitation exists in the various dried samples. The bands shown by the $CuMnO_x$-1 and $CuMnO_x$-3 samples synthesized with Na_2CO_3 as a precipitant are similar. Likewise, bands shown by the $CuMnO_x$-2 and $CuMnO_x$-4 samples prepared with NaOH as a precipitant are similar. Some part bands (centered at *ca.* 3500 cm^{-1} and 1060 cm^{-1}) in $CuMnO_x$-1 and $CuMnO_x$-3 are consistent with those of $CuMnO_x$-2 and $CuMnO_x$-4, however the formation of the carbonate species is observed from the two additional bands at 1460 and 862 cm^{-1}. These results suggest that the crystalline phase of $CuMnO_x$-1 and $CuMnO_x$-3 prepared using Na_2CO_3 as a precipitant consist of carbonate species, which are distinct to that of $CuMnO_x$-2 and $CuMnO_x$-4.

TGA curves of the as-prepared dried precipitates (Fig. 9) show that there is a large mass-loss difference between the $CuMnO_x$-1 and $CuMnO_x$-2 samples. The dried $CuMnO_x$-1 shows an additional 17% weight loss over the $CuMnO_x$-2. During the thermal analysis, $CuMnO_x$-1 in air shows three main thermal effects and loses approximately 19% of its mass. The first weight loss stage is assigned to the loss of physically adsorbed water and the decomposition of $Cu_2(OH)_2CO_3$ (from room temperature to 350 °C, 9% weight loss). The second weight loss is considered to be due to the decomposition of $MnCO_3$ (350–490 °C, 6.6% weight loss). Decomposition of carbonates produces water and carbon dioxide, which may play a role in pore forming and thus improve the specific surface area (121 $m^2\ g^{-1}$). The third weight loss is attributed to the loss of lattice oxygen (490–800 °C, 3% weight loss).

With the same crystalline phases, $CuMnO_x$-1 and $CuMnO_x$-3 prepared using the same precipitant (Na_2CO_3) have analogous TGA curves with the exception that $CuMnO_x$-1 has a greater weight loss. The TGA trace for dried $CuMnO_x$-2 is very similar to $CuMnO_x$-4 except for a distinction in weight loss, with two weight loss stages and one weight increase stage from room temperature to 800 °C, with only a *ca.* 2% weight loss overall. The two weight loss stages for $CuMnO_x$-2 could be due to the loss of physically adsorbed water (room temperature to 310 °C, 2.8% weight loss) and the loss of lattice oxygen (620–800 °C, 0.4% weight loss). In addition, the weight increase stage is attributed to the oxidation of $Cu_{2+1}O$ and Mn_3O_4 (310–620 °C, 1.1% weight increases).

Taking the TGA information of dried samples into account, it can be concluded that the combination of precipitant and precursor in the precipitation process influences the compositions dried precipitation and has an effect on the crystalline phases of the catalysts which in turn influences the CO oxidation activity as confirmed by the catalytic testing. The results from TGA, XRD and FT-IR

measurements suggest strongly that the crystalline phase of dried samples prepared with various types of precipitants are all distinct despite being synthesized with the same precursors. These result in a different catalytic performance of the catalysts calcined from the precipitates. The combination of precipitant and precursor in the precipitation process plays a significant role in producing higher activity catalysts.

4. Conclusions

Copper manganese oxides have been synthesized using different precipitants and precursors by a co-precipitation method and their catalytic activity for CO oxidation has been evaluated. The combination of precipitant and precursor in the reaction has been studied. NaOH as a precipitant resulted in the formation of $Cu_{2+1}O$ and Mn_3O_4 crystals during drying which were converted to a $Cu_{1.5}Mn_{1.5}O_4$ catalyst after calcination at 300 °C. However, Na_2CO_3 as a precipitant resulted in the synthesis of a catalyst mainly consisting of Mn_2O_3 and CuO with higher surface area and catalytic activity for CO oxidation. Using acetate as the precursor in combination with the sodium carbonate precipitant gave the CO oxidation catalyst with the greatest activity. Maintaining the same precipitant while changing the precursor causes a change in the quantity of active sites which influences the CO oxidation activity. The precipitant shows the greatest influence on the crystalline phases of the catalyst while the precursor shows a greater effect on the amount of catalytic active sites which are directly related to the CO oxidation activity. The choice of precipitant and the precursor is important in designing the most efficient CO oxidation catalyst.

Acknowledgments

The project was supported by the National Natural Science Foundation of China (No. 20973031), the Program for New Century Excellent Talents in University of China (NCET-08-0075 and NCET-09-0254), and the Ph.D. Programs Foundation (20100041110017) of Ministry of Education of China.

References

[1] E.C. Njagi, C.H. Chen, H. Genuino, H. Galindo, H. Huang, S.L. Suib, Appl. Catal. B: Environ. 99 (2010) 103–110.
[2] O.Z. Didenko, G.R. Kosmambetova, P.E. Strizhak, J. Mol. Catal. A: Chem. 335 (2011) 14–23.
[3] A.F. An, A.H. Lu, Q. Sun, J. Wang, W.C. Li, Gold Bull. 44 (2011) 217–222.
[4] R.R. Zhang, L.H. Ren, A.H. Lu, W.C. Li, Catal. Commun. 13 (2011) 18–21.
[5] M. Souza, N. Ribeirob, M. Schmal, Int. J. Hydrogen Energy 32 (2007) 425–429.
[6] D. Gamarra, C. Belver, M. Fernández-García, A. Martínez-Arias, J. Am. Chem. Soc. 129 (2007) 12064–12065.
[7] L.C. Wang, L. He, Y.M. Liu, Y. Cao, H.Y. He, K.N. Fan, J.H. Zhuang, J. Catal. 264 (2009) 145–153.
[8] Y. Yu, T. Takei, H. Ohashi, H. He, X. Zhang, M. Haruta, J. Catal. 267 (2009) 121–128.
[9] M. Haruta, T. Kobayashi, H. Sano, N. Yamada, Chem. Lett. 2 (1987) 405–408.
[10] A.S.K. Hashmi, G.J. Hutchings, Angew. Chem. Int. Ed. 45 (2006) 7896–7936.
[11] A. Grirrane, A. Corma, H. Garcia, Science 322 (2008) 1661–1664.
[12] Z. Zou, M. Meng, Q. Li, Y. Zha, Mater. Chem. Phys. 109 (2008) 373–380.
[13] A. Hugon, L. Delannoy, C. Louis, Gold Bull. 42 (2009) 310–320.
[14] B.L. Moroz, P.A. Pyrjaev, V.I. Zaikovskii, V.I. Bukhtiyarov, Catal. Today 144 (2009) 292–305.
[15] H.Y. Lin, Y.W. Chen, Ind. Eng. Chem. Res. 44 (2005) 4569–4576.
[16] K. Qian, S. Lv, X. Xiao, H. Sun, J. Lu, M. Luo, W. Huang, J. Mol. Catal. A: Chem. 306 (2009) 40–47.
[17] B. Lamb, W.C. Bray, J.C.W. Frazer, J. Ind. Eng. Chem. 12 (1920) 213–221.
[18] P.O. Larsson, A. Andersson, Appl. Catal. B: Environ. 24 (2000) 175–192.
[19] J. Li, P. Zhu, R. Zhou, J. Power Sources 196 (2011) 9590–9598.
[20] M.H. Kim, K.H. Cho, C.H. Shin, S.E. Kang, S.W. Ham, Korean J. Chem. Eng. 28 (2011) 1139–1143.
[21] Y. Tanaka, T. Utaka, R. Kikuchi, T. Takeguchi, K. Sasaki, K. Eguchi, J. Catal. 215 (2003) 271–278.
[22] M. Gupta, J.J. Spivey, Catal. Today 147 (2009) 126–132.
[23] M. Li, D. Wang, X. Shi, Z. Zhang, T. Dong, Sep. Purif. Technol. 57 (2007) 147–151.
[24] C. Jones, S.H. Taylor, A. Burrows, M.J. Crudace, C.J. Kiely, G.J. Hutchings, Chem. Commun. 14 (2008) 1707–1709.
[25] V.H. Vu, J. Belkouch, A. Ould-Dris, B. Taouk, J. Hazard. Mater. 169 (2009) 758–765.
[26] M.R. Morales, B.P. Barbero, L.E. Cadús, Fuel 87 (2008) 1177–1186.
[27] D.R. Merrill, C.C. Scalione, J. Am. Chem. Soc. 43 (1921) 1982–2002.
[28] G. Fortunato, H.R. Oswald, A. Reller, J. Mater. Chem. 11 (2001) 905–911.
[29] Y.I. Hasegawa, R.U. Maki, M. Sano, T. Miyake, Appl. Catal. A: Gen. 371 (2009) 67–72.
[30] Y. Hasegawa, K. Fukumoto, T. Ishima, H. Yamamoto, M. Sano, T. Miyake, Appl. Catal. B: Environ. 89 (2009) 420–424.
[31] Z.R. Tang, C.D. Jones, J.K.W. Aldridge, T.E. Davies, J.K. Bartley, A.F. Carley, S.H. Taylor, M. Allix, C. Dickinson, M.J. Rosseinsky, J.B. Claridge, Z. Xu, M.J. Crudace, G.J. Hutchings, ChemCatChem 1 (2009) 247–251.
[32] G.J. Hutchings, A.A. Mirzaei, R.W. Joyner, M.R.H. Siddiqui, S.H. Taylor, Appl. Catal. A: Gen. 166 (1998) 143–152.
[33] A.A. Mirzaei, H.R. Shaterian, M. Habibi, G.J. Hutchings, S.H. Taylor, Appl. Catal. A: Gen. 253 (2003) 499–508.
[34] C. Jones, K.J. Cole, S.H. Taylor, M.J. Crudace, G.J. Hutchings, J. Mol. Catal. A: Chem. 305 (2009) 121–124.
[35] A.A. Mirzaei, H.R. Shaterian, M. Kaykhaii, Appl. Surf. Sci. 239 (2005) 246–254.
[36] S.B. Kanungo, J. Catal. 58 (1979) 419–435.
[37] S. Verprek, D.L. Cocke, S. Kehl, H.R. Oswald, J. Catal. 100 (1986) 250–263.
[38] F.C. Buciuman, F. Patcas, T. Hahn, Chem. Eng. Process. 38 (1999) 563–569.
[39] M. Krämer, T. Schmidt, K. Stöwe, W.F. Maier, Appl. Catal. A: Gen. 302 (2006) 257–263.
[40] P.T. Tanev, T.J Pinnavaia, Chem. Mater. 8 (1996) 2068–2079.
[41] K. Morgan, K.J. Cole, A. Gogueta, C. Hardacre, G. Hutchings, N. Maguire, S. Shekhtman, S. Taylor, J. Catal. 276 (2010) 38–48.
[42] M. Luo, Y. Zhong, X. Yuan, X. Zheng, Appl. Catal. A: Gen. 162 (1997) 121–131.
[43] B. Solsona, T. Garcia, S. Agouram, G.J. Hutchings, S.H. Taylor, Appl. Catal. B: Environ. 101 (2011) 388–396.
[44] H. Chen, X. Tong, Y. Li, Appl. Catal. A: Gen. 370 (2009) 59–65.
[45] B. Wu, L. Tian, H. Xiang, Z. Zhang, Y.W. Li, Catal. Lett. 102 (2005) 211–218.
[46] S.A.C. Carabineiro, S.S.T. Bastos, J.J.M. Órfaõ, M.F.R. Pereira, J.J. Delgado, J.L. Figueiredo, Catal. Lett. 134 (2010) 217–227.
[47] K. Zhi, Q. Liu, Y. Zhang, S. He, R. He, J. Fuel Chem. Technol. 38 (2010) 445–451.